Parameter optimization in jet flow control

By Angela Hilgers

1. Motivation and objectives

The control of turbulent jet flows has applications in combustion, aerodynamic noise, and jet propulsion. In combustion processes it is important to enhance the turbulent mixing of the chemical species to make the process more efficient and reduce the concentration of pollutants. Acoustic emission of an aircraft can be reduced by controlling flow unsteadiness that produces noise. Enhanced mixing in aircraft propulsion systems decreases the plume temperature and suppresses infrared radiation.

The mixing rate of a turbulent jet can be significantly altered by applying a suitable excitation at the jet orifice. Various experiments have been carried out to study the reaction of jets to external forcing (Crow 1971, Ho 1982, Lee 1985, Parekh 1987, Parekh 1988). It has been shown that a large spreading of the jet can be achieved with a small mass flow actuation if suitable frequencies are chosen (Parekh 1996). Here, it is assumed that a large spreading angle corresponds to efficient mixing of a passive scalar transported by the flow with the surrounding air. Numerical simulations of compressible and incompressible jet flows have been carried out that confirm many observations made in experiments with periodically forced jets (Freund 1998, Freund 1999, Danaila 1998, Urbin 1997). An automatic search for optimal actuation parameters was carried out by Koumoutsakos *et al.* 1998. This work showed that evolution strategies are capable of finding suitable actuations for a vortex model and direct numerical simulations of compressible jets.

In this paper we compare the effects of helical and combined axial and helical forcing on a jet. We combine evolution strategies with direct numerical simulation (DNS) to search for the actuation parameters that maximize the spreading of the jet. An objective function that measures the spreading of the jet evaluates the performance of a given set of actuation parameters. The evolution strategy searches for the optimal actuation by automatically varying the parameters and calculating their objective function value. Solutions that lead to a pronounced spreading are found within reasonable time although the evaluation of the objective function, the DNS of the jet, is expensive. It has been shown in experiments that jet mixing can be significantly enhanced by using dual-frequency actuation (Parekh & Reynolds 1987, 1988). Our simulations confirm that a combined axial and helical actuation is much more efficient with respect to jet mixing than a helical actuation alone.

2. Accomplishments

2.1 Numerical method

The numerical solver simulates a free round jet issuing from a circular orifice of diameter D in a solid wall. The incompressible Navier-Stokes equations and

the transport equation for a passive scalar are solved in a spherical coordinate system, with (r, θ, ϕ) denoting the radial, tangential, and azimuthal directions. The computational domain is bounded in the radial direction by the surfaces $r = 5D$ and $r = 15D$ and by the cone starting from the center of the sphere with an opening angle of 36^o. This geometry covers a domain with a streamwise extent of $10D$ and a spanwise diameter of $4D$ for the inflow section and $10D$ for the outflow section. Such a discretization is able to follow the streamwise spreading of the jet and allows a well-balanced resolution of the flow field with a reasonable number of grid points. Spatial derivatives are calculated on a staggered spherical grid. The time integration is carried out with a second order Adams-Bashforth method. More details of the numerical scheme can be found in Boersma (1998).

At the lateral boundary, the total normal stress is set to zero, which allows fluid exchange across the boundary. This condition properly simulates the entrainment of ambient fluid in the spreading jet flow. A so-called convective boundary condition (Orlanski 1976) is used to evacuate the vortex structures through the downstream boundary. At the inflow section, the mean streamwise velocity profile is imposed as initial and boundary condition

$$V_{z0}(r_c) = \frac{V_0}{2}\left(1 + tanh\Big[0.25D/\Theta_0(D/(4r_c) - 4r_c/D)\Big]\right), \tag{1}$$

where V_0 is the centerline velocity and r_c is the radius in a *cylindrical system*. The initial momentum thickness was $\Theta_0 = D/60$ in our simulations.

For the DNS of a jet with $Re = 1500$, based on orifice velocity V_0 and diameter D, the spherical grid consists of $192 \times 128 \times 96$ points in the radial, tangential, and azimuthal direction. Typical CPU times for the calculation of a fully developed jet are 1500 node hours on an Origin 2000, using the Message Passing Interface (MPI). Optimization requires the simulation of approximately 150 jets for different actuation parameters. We will explain in Sec. *2.3* how we have reduced the CPU time during the optimization process.

In unforced jets, large coherent structures are observed that are related to the instability modes of the jet. The dominating modes are the axisymmetric or varicose mode and helical modes. The axisymmetric mode causes the shear layer to roll up into vortex rings. By applying axial forcing to the shear layer, the frequency of vortex ring generation and the pairing of the vortex rings may be altered.

The initial shear layer is able to amplify a large range of frequencies. The frequency which leads to the maximum amplification of the initial shear layer is called the natural frequency. It can be obtained by linear spatial instability analysis (Michalke 1984, Ho & Huerre 1984). For an axisymmetric jet with initial velocity profile (1), it is $St_\Theta = f\Theta/V_0 = 0.018$. The natural frequency is lower for thicker shear layers, as they appear in forced jets. The frequency f_p of the axial perturbation that produces the largest total amplification is called the preferred mode of the jet. It corresponds to the frequency of vortices at the end of the potential core. This frequency has been determined to be $St_p \approx 0.3$ (Crow 1971, Hussain 1981). However, other studies have found the preferred Strouhal number to vary

between 0.25 and 0.5 (Hussain 1981). Mankbadi (1985) observed for a round jet under axisymmetric forcing that mixing is enhanced if the forcing Strouhal number corresponds to about twice the jet's preferred mode. It was also found that at high Strouhal numbers the momentum thickness is reduced along the jet.

Mixing may be increased significantly if axial and helical forcing are combined (Lee 1985, Parekh 1987, Parekh 1997). In the following we will denote the Strouhal numbers of axial and helical forcing with St_a and St_h. Large spreading angles (up to 80°) have been observed for certain ratios $\beta = St_a/St_h$ of the Strouhal numbers (Parekh 1988). In particular, the jet splits into two branches for $\beta = 2$ (bifurcating jet) and into three branches for $\beta = 3$. For non-integer ratios $1.6 < \beta < 3.2$, vortex rings are shed in various radial directions (blooming jet). It has been discussed by Parekh & Reynolds (1988) that these flow patterns appear for both low and high Reynolds numbers.

In our simulation the actuation of the shear layer was achieved by superposing periodic disturbances on the initial velocity profile. We have used two kinds of actuation. For the first, the total inflow velocity in the z direction of a cylindrical coordinate system (z, r_c, φ) is

$$V_z(r_c, \varphi, t) = V_{z0}(r_c) \left[1 + A_h sin \left(2\pi St_h \frac{V_0}{D} \right) cos(\varphi) \frac{2r_c}{D} \right]. \tag{2}$$

A_h is the amplitude of the actuation, which is phase locked in the plane $\varphi = 0$. It corresponds to the superposition of two counter rotating helical modes of the same frequency. It has been observed in simulations and experiments that this type of actuation causes the jet to perform a flapping motion in the plane of actuation. The second type of actuation is a superposition of axial and helical modes

$$V_z(r_c, \varphi, t) = V_{z0}(r_c) \left[1 + A_a sin \left(2\pi St_a \frac{V_0}{D} t \right) + A_h sin \left(2\pi St_h \frac{V_0}{D} t + \alpha \right) cos(\varphi) \frac{2r_c}{D} \right]. \tag{3}$$

Here A_a and A_h are the amplitudes of the axial and helical mode and St_a, St_h are the respective Strouhal numbers. We have again chosen the helical part of the actuation to be phase-locked in the plane $\varphi = 0$. The angle α determines the plane of spreading. The actuation (2) with $\beta = St_a/St_h = 2$ has been used before to model bifurcating jets (Danaila 1998). To simplify the notation, we will refer to jets obtained with the dual-frequency actuation equation (3) as bifurcating jets, even if β takes on a value that is not exactly two. In the following sections we will investigate for which parameter vector $\mathbf{x} = (St_a, St_h, A_a, A_h)$ the spreading of the jet is maximal.

2.2 Optimization with evolution strategies

Evolutionary computation techniques use the basic principles of evolution: a reproduction cycle, natural selection, and diversity by variation, to find the optimal solution to a given problem. The phase space of possible actuation parameters is searched automatically by an evolution strategy. There have been numerous

applications of evolution programs in engineering, which is due to the simplicity of these strategies and their robustness. It has been shown by Koumoutsakos *et al.* (1998) that evolution strategies are well suited for the optimization of jet actuation since they are easy to implement, inherently parallel, and very efficient.

An optimization problem is described by a set, or vector, of parameters that are varied during the procedure and an objective or fitness function that evaluates the performance of the parameters. The surface that describes the fitness value as a function of the parameters is referred to as fitness landscape. While classical approaches like gradient methods converge quickly, there is a certain risk of premature convergence to a local optimum. Stochastic methods, on the other hand, avoid this by allowing steps in seemingly unfavorable directions with a certain probability. They are, therefore, useful for the optimization of multimodal functions. The dynamic behavior of the jet is determined by the nonlinear interaction of different modes. This is likely to cause a complicated dependence of the jet development on the actuation parameters. We therefore expect the objective function to be multimodal, which makes the use of stochastic optimization methods necessary.

Evolution strategies describe populations of individuals which represent possible solutions of the given problem. Each individual represents a vector $\mathbf{x}$ containing n parameters and an associated vector $\mathbf{s}$ containing n mutation steplengths. In the simplest possible case, each generation consists of only one parent and one offspring. An offspring is obtained from the parent by a random mutation

$$\mathbf{x}_o^{i+1} = \mathbf{x}_p^i + \mathbf{s}_p^i N(0,1). \tag{4}$$

Here the indices p and o denote parent and offspring and i is the number of the generation. $N(0,1)$ is a normal distribution with zero average and unit variance. The performance of the offspring is evaluated by the objective function. Depending on the objective function value, the parent is kept for the next generation or replaced by the offspring.

For optimization problems with multimodal fitness landscapes, the search of the parameter space can be sped up by simultaneously evaluating several search trajectories. This corresponds to evolving generations with several parents and offspring. We have used an evolution strategy with μ parents and λ offspring, where in each generation the best μ individuals are chosen among the $\mu + \lambda$ parents and offspring ($(\mu + \lambda)$ strategy).

The steplengths of the mutation are decreased if the offspring are better than the parents, otherwise they are increased. For the $(1 + 1)$ strategy this is done according to the 1/5 success rule (Rechenberg 1994); for the $\mu + \lambda$ strategy either the steplengths of successful mutations are passed on to the next generation or the Covariance Matrix Adaptation of the step size (CMA, Hansen 1996, Koumoutsakos 1999) is used, which takes into account not only successful mutations of the previous generation, but the whole path the evolution has taken. There are certain limits to the parameters. The amplitudes must be positive, and the Strouhal numbers should be within a certain interval. When a mutation step leads to a value outside the allowed range, the step is considered unsuccessful and is repeated until allowed values are obtained.

2.3 Jet optimization

An important part of the formulation of the optimization problem is the choice of an objective or fitness function which measures the spreading of the jet and is sufficiently sensitive to changes in the actuation parameters. Furthermore, we have to ensure that the evaluation of the objective function is possible within reasonable CPU times.

The objective function must be based on the quantities calculated by the DNS simulation: the velocity field, the scalar concentration, and the pressure. The dependence of the radial velocity on the actuation parameters is pronounced while the variation of the axial and azimuthal velocity is small and difficult to quantify. We have, therefore, maximized the integral of the radial velocity (in the cylindrical system)

$$f(\mathbf{x}, t_0) = \int_V v_{r_c}^2(r, \theta, \varphi, t_0) dV' \tag{5}$$

where V is the whole computational domain. The integral of $v_{r_c}^2$ is time dependent. A suitable time t_0 must be chosen in the jet simulation for the evaluation of the objective function.

Other possible objective functions are the centerline velocity or the spreading angle of the jet. The spreading angle, which has been used as objective function in Koumoutsakos (1998) in the simulation of inviscid vortex rings, is difficult to quantify in our simulations because pressure rings are not well resolved far away from the orifice. While the integral of v_r^2 changes as a function of the parameter values early in the DNS, the center line velocity does not show clear variations at that stage. Different objective functions have been investigated by Freund & Moin (1999). It has been shown that volume integrals of moments of the scalar concentration and integrals of the scalar dissipation are suitable metrics to quantify mixing in a jet.

Figure 1 shows how the objective function $f(\mathbf{x}, t)$ evolves with time for the single-frequency actuation equation (2). The three curves correspond to different values of the Strouhal number at constant amplitude $A_h = 0.05$. The time scale is the normalized scale of the jet simulation. (For comparison, the time scale of an excitation with $St = 0.55$ is $T = D/(StV_0) = 0.29$, and for $St = 0.36$ it is $T = 0.44$. The time for the DNS of a fully developed jet is approximately $t = 7$.) We have determined the fitness value of the parameter vector at time $t_0 = 1.6$ where the objective function values already clearly differ. In Fig. 1, the objective function is shown for the Strouhal number $St = 0.36$ that maximizes the objective function value at $t = 1.6$ and for $St = 0.17$ and $St = 0.55$ that resulted in much lower values. For $St = 0.55$, the spreading of the jet starts later and reaches lower values; for $St = 0.17$ the overall spreading is low. For Strouhal numbers in the vicinity of the optimal Strouhal number, the fitness value is only slightly smaller than the maximum value. Which Strouhal number from this region is chosen as the global optimum may depend on the choice of the time t_0.

In order to further decrease the computational time for the optimization, we have used a coarse grid with $64 \times 64 \times 32$ grid points. Although most of the structures

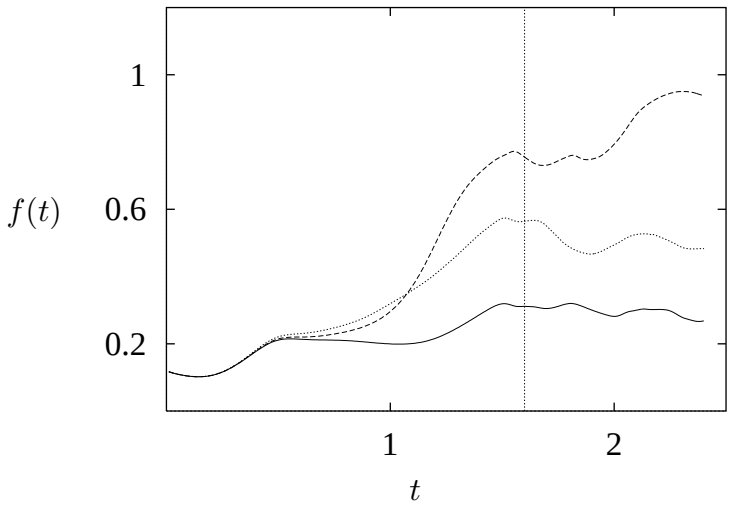

FIGURE 1. Objective function f vs. time for a jet forced with single-frequency excitation (2) and $A_h = 0.05$, $St = 0.17$ (———), $St = 0.36$ (- - - -), $St = 0.55$ (·····); the fitness value is determined at $t = 1.6$.

observed in the jet are not resolved on this grid, the objective function shows a very similar behavior as a function of time in the early stages of the simulation. With this approximation, the CPU time necessary for one evaluation of the objective function is approximately 3 node hours on a SGI-ORIGIN 2000. The data shown in Fig. 1 have been obtained from simulation on this coarse grid. We note that under-resolved simulations can only be used for a rough estimate of the jet dynamics. In addition, it cannot be excluded that $f(t)$ curves corresponding to different parameters may cross at times $t > t_0$. However, by comparing $f(t)$ for different grid resolutions and by relating jet spreading at time t_0 with the full jet simulation, we found the approximations made do not significantly affect the results. In fact, our approach leads to good results while keeping the computational time within reasonable limits.

For the data shown in Fig. 1, the jet simulation has been started at time $t = 0$ from the initial laminar flow at the orifice. The optimization has been repeated with an initial non-laminar velocity field, which has been obtained from a jet simulation with small axial and random forcing. The parameter vectors found by the evolution strategy again did not differ significantly.

Figure 2 shows the fitness value as a function of the generation number. The optimization has been done for the dual-frequency actuation (3) by varying two parameters $\mathbf{x}_0 = (St_a, \beta)$. The amplitudes have been kept constant at $A_a = 0.025$ and $A_h = 0.05$ and the fitness function (5) has been evaluated at $t_0 = 1.6$. Starting from an initial vector $\mathbf{x}_0 = (0.5, 2.5)$ the best spreading was obtained after 30 generations for the parameters $\mathbf{x}_{best} = (0.66, 2.1)$. In Fig. 2 the fitness value shown is the average of the two best individuals rather than the single best. This causes the non-monotonic behavior including the dips around the 10th and at the 18th generation. For the initial value chosen here the vicinity of the optimum is reached by the best individual already after a few generations. In general the search needs

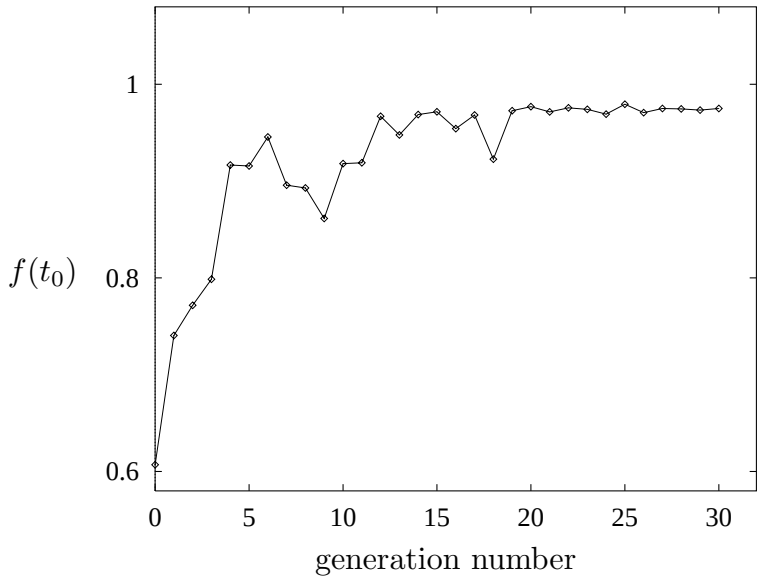

FIGURE 2. Convergence of the evolution strategy for the parameter vector $\mathbf{x} = (St_a, \beta)$ and $A_a = 0.025$, $A_h = 0.05$ fixed.

to be continued for a larger number of generations to ensure that convergence to a local optimum is avoided.

2.4 Results of the optimization

The limits of the Strouhal numbers were $0.1 < St_h < 0.55$ for the single-frequency and $0.1 < St_a < 1.2$ for the dual-frequency excitation. For the latter case, the ratio of Strouhal numbers was $1.6 < \beta < 3.2$. This corresponds to the range used in experiments with bifurcating jets.

We first varied only the Strouhal number of the actuation equation (2) and kept the amplitude A_h fixed. The optimization was done with the objective function (5) and the $(1 + 1)$ evolution strategy. Starting from an initial value $St = 0.5$, the evolution path was found to approach an optimum in the 27th generation (28 evaluations of the fitness function) at $St = 0.36$. Our computations have shown that the optimization strategy tends to choose the amplitude to be as large as possible within the given limit. Since an actuation with very large amplitudes is not desirable, we have kept $A_h = 0.05$ fixed for the single-frequency actuation.

We repeated the calculation with an objective function that integrates v_r^2 within the subdomain between 5 and 10 jet diameters from the nozzle. This neglects spreading in the part of the computational domain close to the orifice and, therefore, favors lower Strouhal numbers. As a result of the optimization, we found $St = 0.28$. While Parekh *et al.* found the most intense motion of the jet for $St \approx 0.2$, they also observed efficient mixing at $St \approx 0.27$, which is close to our result, and at $St \approx 0.4$.

The fitness value is shown as a function of the Strouhal number in Fig. 3 for the two cases: the evaluation of the objective function (5) in the whole domain and in half the domain. The location of the extrema of the fitness landscape depends on the domain chosen. For the latter case there is only one maximum at $St = 0.28$. For

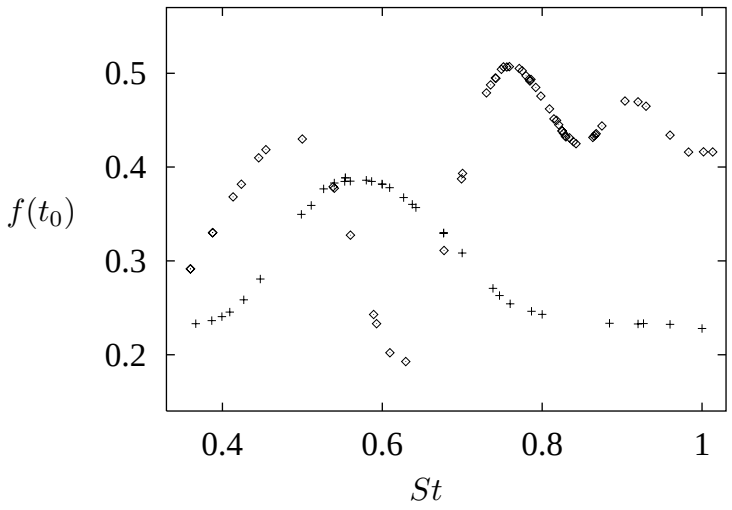

FIGURE 3. Fitness value as function of the Strouhal number for evaluation of the integral (5) over the whole (rhombs) and half (crosses) of the computational domain.

the large domain we have found the global maximum at $St = 0.36$, and there are local maxima at $St = 0.24$ and $St = 0.45$. In this case the evolution strategy is able to find the global maximum independent of the starting value. For low Strouhal numbers the mode that determines the creation of vortices saturates and is replaced by its subharmonic further downstream than for large Strouhal numbers. The first pairing of vortices, which is the onset of the jet spreading, happens further away from the orifice for small Strouhal numbers. Evaluation of the objective function in half of the domain as described above, therefore, favors lower Strouhal numbers.

For the best Strouhal numbers found by the evolution strategy, we have repeated the DNS of the jet on the fine grid described in section 2.1. Figure 4 shows the passive scalar concentration obtained when the helical actuation (Eq. 2) is applied at the orifice. It is a snapshot taken at time $t = 9$ (based on the normalized time scale of the jet). Different shades of grey denote different concentration C of the scalar. The concentration is approximately one in the inner (dark) region and zero far outside (white) region. The figure shows the jet in the plane of the actuation, $\varphi = 0$ (left), and in the plane $\varphi = \pi/2$ (right). The jet spreads rapidly in the plane of the actuation and contracts in the orthogonal plane. Although the amplitude of the actuation is small, the jet spreads at a large angle, and the jet column shows a strong flapping motion. The jet column disintegrates towards the end of the computational domain, but regions of concentration $C \approx 1$ remain near the centerline of the jet. Figure 5 shows the best result obtained using half of the computational domain for the evaluation of the fitness function. The jet spreads further downstream from the orifice than in the previous case.

Instead of keeping the amplitude fixed during the optimization, we have also used an objective function that penalizes large amplitudes $f_{penalty}(\mathbf{x}) = f(\mathbf{x}) - CA_h^2$ with $C > 0$, which seeks to maximize the spreading of the jet while minimizing

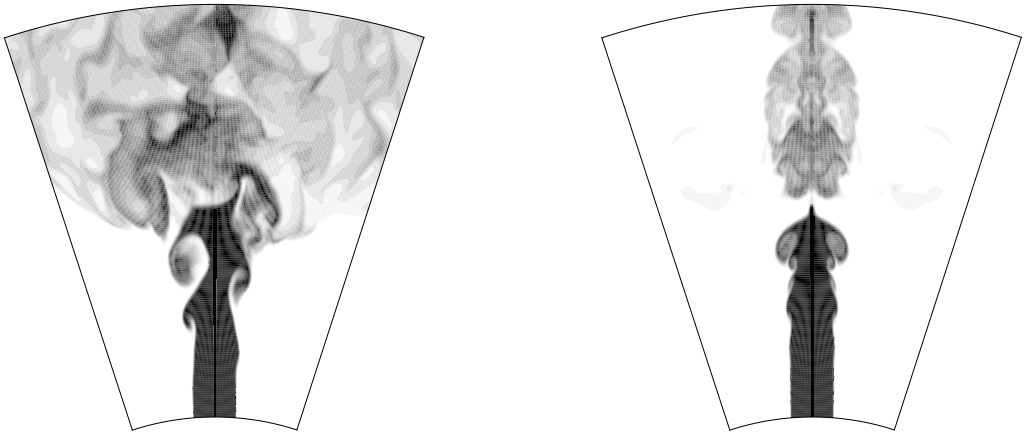

FIGURE 4. Snapshots of the passive scalar concentration at time $t = 9$ for a jet excited with the single-frequency actuation (Eq. 2) in the plane of the actuation $\varphi = 0$ (left) and the plane $\varphi = \pi/2$ (right); $St = 0.036$ and $A_h = 0.05$.

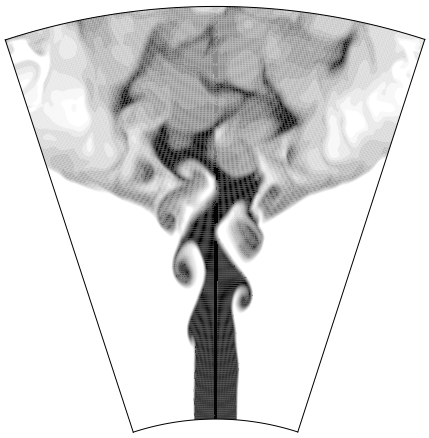

FIGURE 5. Snapshot of the scalar concentration at time $t = 7$ for a jet actuated with single-frequency actuation (Eq. 2) and $St_h = 0.28$, $A_h = 0.075$.

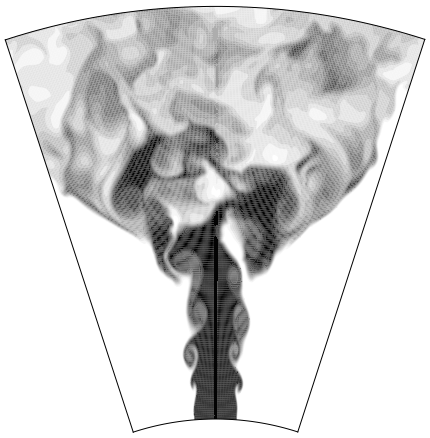

FIGURE 6. Snapshot of the scalar concentration at time $t = 7$ for a jet actuated with dual-frequency forcing (Eq. 3) and $St_a = 0.66$, $St_h = 0.31$, $A_a = 0.025$, $A_h = 0.075$.

the amplitude A_h. The constant C is chosen such that the two terms are of the same order of magnitude. The optimization with this objective function (where the integral is again calculated over the whole computational domain) produced $\mathbf{x} = (St_h, A_h) = (0.29, 0.08)$ as best parameter values. Details of the optimization using a penalty function are described in (Hilgers 1999).

For the two-frequency actuation we have varied the two Strouhal numbers and one of the amplitudes. The second amplitude was kept fixed in order to reduce the dimension of the search space. We did the following optimization runs.

1. Variation of $\mathbf{x} = (St_a, \beta, A_h)$, with $\beta = St_a/St_h$ for different start vectors and with different evolution strategies: a $(\mu + \lambda)$ strategy with $\mu = 2$ and $\lambda = 5$ and the $(1 + 1)$ strategy,
2. Variation of $\mathbf{x} = (St_a, \beta)$ while keeping both amplitudes fixed,
3. Separate optimization of St_a and (β, A_h).

We will only summarize the main results; details of the optimization procedure are described in Hilgers (1999).

For Cases 1 and 2, the global maximum was found at the same Strouhal numbers $(St_a = 0.66, St_h = 0.31)$. In the first case, the variation of the Strouhal numbers and one amplitude, it was again found that the amplitude was chosen as large as possible within the given limits. While the objective function value grows with the amplitude, variations of A_h do not have a large influence on the *shape* of the fitness landscape. Therefore, the frequencies are the important parameters of the optimization. The amplitudes do not significantly influence the location of the optimum in the space of frequencies within the given parameter range. It has been shown, however, in (Mankbadi 1985) that for axial forcing the Strouhal numbers that enhance mixing are different at very low $(A < 0.01)$ and at high forcing levels.

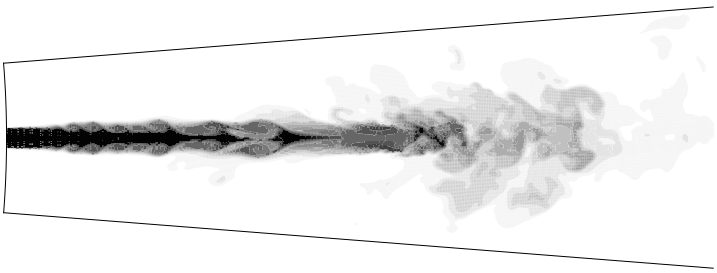

FIGURE 7. Snapshot of the scalar concentration of a natural jet without significant actuation, $Re = 2000$.

The same best parameter vector was found for different start vectors. In some cases the search path started near a local optimum and crossed an area with low objective function values before approaching the global optimum. This shows that the evolution strategies indeed avoid premature convergence to local optima. If a starting point is chosen far away from the optimum, the evaluation of up to 50 generations may be necessary. Figure 6 shows a snapshot of the jet actuated with the parameters $\mathbf{x}_{best} = (St_a, St_h) = (0.66, 0.31)$, $A_h = 0.075$, and $A_a = 0.025$. This dual-frequency actuation leads to an impressive spreading of the jet. The center of the jet shows a strong flapping motion, which is due to the large amplitude of the helical forcing. Comparing Figs. 6, 4, and 5 we find that the shape of the jet differs slightly for the three types of actuation. The overall spreading, i.e. the area, to which a significant amount of the tracer is transported, is comparable, although the total amplitude is smaller for the jets with one-frequency forcing. The flapping motion of the jet column, however, is most pronounced for the dual-frequency actuation. The jet column is completely dispersed near the end of the domain, indicating that the jet bifurcates. Although a clear spreading in two branches is not visible, there are areas on both sides of the centerline with much higher concentration of the scalar and much lower radial velocity (not shown) than on the centerline. For comparison we also show a natural jet, calculated for a slightly higher Reynolds number, in Fig. 7. A larger domain is chosen since the potential core is much longer in this case. The spreading angle of the jet is approximately 10°. A quantitative comparison of the jets obtained by our simulation with the experimental results by Parekh *et al.* (1996) is difficult because the Reynolds numbers differ. In addition, different types of perturbation are used in the experiment and simulation, and hence spreading angles will always be slightly different.

For Case 3, the separate optimization of the frequencies, the resulting optimal parameter vector differs from that of the Cases 1 and 2. The corresponding fitness value is slightly smaller, indicating that the parameter values obtained for simultaneous optimization lead to a larger spreading of the jet. The Strouhal numbers are not independent and should be optimized simultaneously. This result is not

surprising because the spreading pattern of the jet is due to the interaction of the various modes in the jet. For Case 1 we compared the performance of different evolution strategies. We used a $(\mu + \lambda)$ strategy with Covariance Matrix Adaption of the steplength as well as a simple $(1 + 1)$ strategy. We found that the number of objective function evaluations that is necessary to approach the optimum does not differ significantly for these strategies. It should be noted that the convergence speed of the $(1 + 1)$ strategy depends not only on the choice of the initial parameter vector, but also on the initial steplengths. However, the fact that the simple strategy, which uses only one search path, can reach the optimum rapidly indicates that for our optimization problem the landscape is not too complex.

The best actuation parameters found by the different optimization runs are summarized in Table 1. Note that in all except the first case the optimal Strouhal number of the helical actuation is $St \approx 0.3$. It differs from the natural Strouhal number, for which linear instability analysis predicts the largest amplification of signals (Michalke 1984), but is in agreement with the preferred frequency of the jet found by Crow & Champagne (1971). The optimal axial Strouhal number found by the optimization procedure is approximately twice as large as the preferred frequency, as predicted by Mankbadi (1985).

In the formulation of the optimization procedure, some arbitrary choices have been made that may affect the results. The optimal parameter vector depends on the choice of the time, t_0, at which the objective function value is determined. It also depends on the domain that is chosen for the integration of v_r^2 or in general on the length of the computational domain. However, for each choice of the domain, actuation parameters were found that lead to a large spreading of the jet.

type of actuation	St_a	St_h	A_a	A_h
single-freq., Eq. (2)	–	0.36	–	0.05 (fixed)
single-freq., penalty $C = 5$	–	0.29	–	0.08
two-freq., Eq. (3)	0.66	0.31	0.025 (fixed)	0.075
two-freq., separate opt. of St_i	0.72	0.29	0.025 (fixed)	0.075 (fixed)

Table 1. Best actuation parameters found by the evolution strategies.

2.5 Mean flow

In the previous section we have shown that the spreading of the jet strongly depends on the forcing applied in the inflow plane. The average streamwise velocity and concentration of the scalar on the centerline of the jet is evaluated in order to obtain a more quantitative measure of turbulent mixing. From turbulence theory it is known that the decay rate of round jets is proportional to $[z-z_0]^{-1}$ where z_0 is the virtual origin of the jet and z the distance measured from the jet orifice (Schlichting 1979). The perturbations given by Eqs. (2) and (3) are not axisymmetric, and, therefore, linear decay of the jet is not expected. In Fig. 8 (left) we show the centerline velocity obtained from the flapping and bifurcating jet computations.

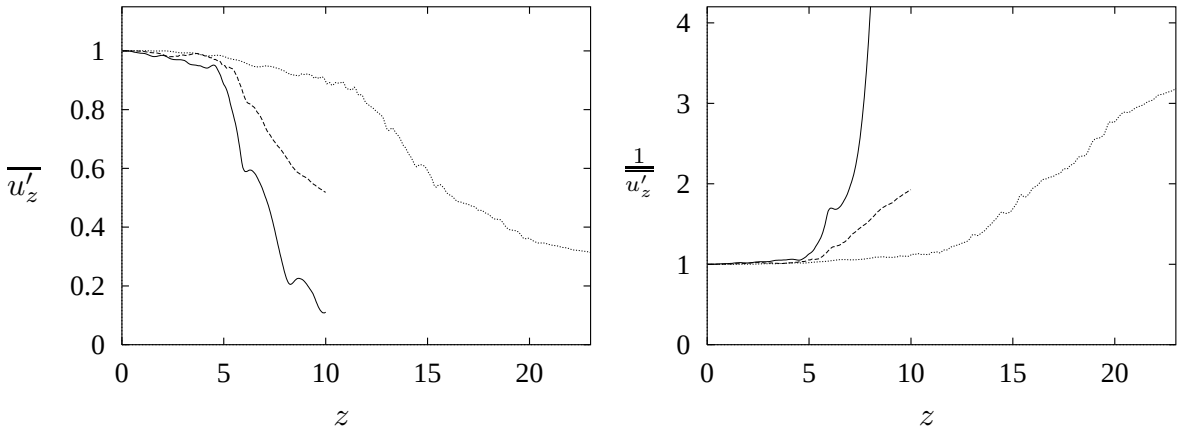

FIGURE 8. The averaged centerline velocity $\overline{u'_z}$ (left) and the inverse of the centerline velocity (right) for the bifurcating (——), flapping (– – – –) and standard (·····) jets.

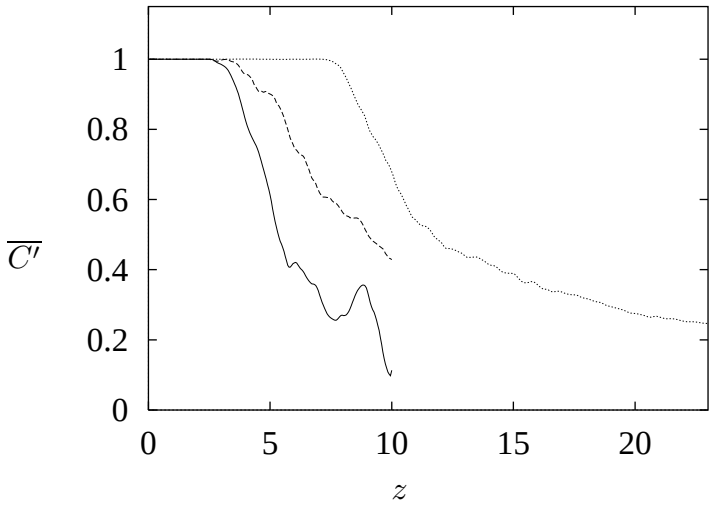

FIGURE 9. The averaged streamwise centerline scalar concentration $\overline{C'}$ for the bifurcating (——), flapping (– – – –) and standard (·····) jets.

For comparison we include the profile for a round axisymmetric jet (standard jet) with comparable Reynolds number. For both the flapping and bifurcating jets, the centerline velocity starts to drop near $z/D = 5$, which is much earlier than in the standard jet. The decay rate (slope of the curve in Fig. 8, right) of the flapping jet is comparable to that of the standard jet while the bifurcating jet decays much faster. For the flapping jet the decay is approximately linear, for the bifurcating jet superlinear.

In our simulation it can be assumed that for values of the scalar concentration $C \approx 0.5$ the flow is well mixed. In Fig. 9 we show the center line scalar concentration for the bifurcating, the flapping, and the natural jet. The actuation leads to a much earlier decay of the concentration than for the natural jet. For the flapping

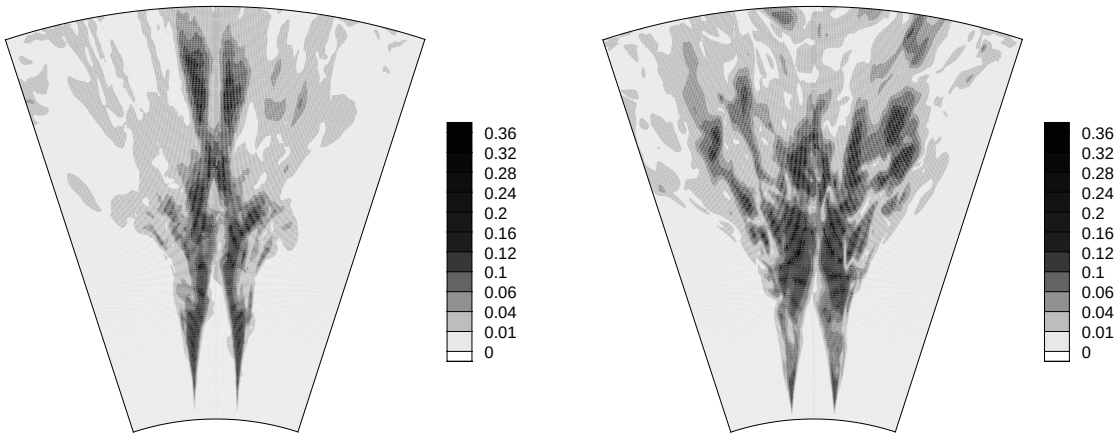

FIGURE 10. The norm of the turbulent scalar flux $\sqrt{\overline{u_r'C'}^2 + \overline{u_z'C'}^2}$ for the flapping (left) and bifurcating (right) jets in the plane of the actuation.

actuation, the concentration reaches $C \approx 0.4$ on the centerline at the end of the domain. For the bifurcating jet, the decay starts even earlier and the mixing is very efficient. Towards the end of the domain, the average of the concentration reaches low values due to the bifurcation of the jet, which transports the scalar away from the centerline. Fig. 10 shows the total turbulent flux of the scalar $\sqrt{\overline{u_r'C'}^2 + \overline{u_z'C'}^2}$ in the plane of the actuation for both the flapping and bifurcating jets. For the flapping jet the flux has high values near the centerline. The bifurcating actuation on the other hand directs the total flux outwards. The bifurcating jet, therefore, has by far the best mixing properties. From the figures presented in this section, it is clear that there is a certain amount of scatter in the DNS data due to the limited size of the statistical sample.

3. Summary and future plans

DNS and evolution strategies have been combined to search for actuation parameters (Strouhal numbers and amplitudes) that enhance mixing in a jet. The main result is that a combined axial and helical perturbation leads to better mixing and a faster decay of the center line velocity and scalar concentration than a flapping perturbation, as has been shown before in experiments by Parekh *et al.* (1987). For applications it is necessary to have a large spreading not only in one plane, but in the whole three-dimensional domain. This can be obtained by replacing the phase-locked helical forcing used in our simulation by a helical actuation that is rotating around the orifice.

The evolution strategies appear to be very efficient for optimization of the jet actuation. Although convergence to a local optimum can never be completely excluded, it can be stated that the strategy is able to find a good solution within reasonable time. In a real experiment the perturbation is not described by a simple

mathematical function like in our simulation, and, therefore, a one-to-one comparison between simulation and experiment is difficult. However, we expect that the frequency range found to be best in our simulations is similar to that for experiments under comparable conditions. We also expect that evolution programs can be used to optimize physical experiments. Future work will concentrate on the use of more realistic actuators and on simulations at higher Reynolds numbers.

Acknowledgments

The author is grateful to B. Boersma for providing the DNS code and for valuable discussions throughout this work. She wishes to thank S. Müller and P. Koumoutsakos for kindly providing their evolution strategy programs and for many discussions on optimization problems. Support from the US Air Force Office of Scientific Research and the Boeing Company is gratefully acknowledged.

REFERENCES

Boersma, B. J., Brethouwer, G., & Nieuwstadt, F. T. M. 1998 A numerical investigation on the effect of the inflow conditions on a self-similar region of a round jet. *Phys. Fluids* **10**, 899-909.

Crow, S. C. & Champagne, F. H. 1971 Orderly structures in jet turbulence. *J. Fluid Mech.* **48**, 547-591.

Danaila, I. & Boersma, B. J. 1998 Mode interaction in a forced homogeneous jet at low Reynolds numbers. *Proceedings of the 1998 Summer Program*, Center for Turbulence Research, NASA/Stanford Univ., 141-158.

Freund, J. B. & Moin, P. 1998 Mixing enhancement in jet exhaust using fluidic actuators: direct numerical simulations. *ASME* FEDSM98-5235.

Freund, J. B. & Moin, P. 1999 Jet mixing enhancement by high amplitude fluidic actuation. in preparation.

Hansen, N. & Ostermeier, A. 1996 Adapting arbitrary normal mutation distributions in evolution strategies: the covariance matrix adaptation. *Proceedings of the IEEE International Conference on Evolutionary Computation (ICEC'96),* 312-317.

Hilgers, A., Müller, S. M., Boersma, B. J., & Koumoutsakos, P. D. 1999 Turbulent jet mixing optimization with evolution strategies. In preparation.

Ho, C.-M. & Huang, L. S. 1982 Subharmonics and vortex merging in mixing layers. *J. Fluid Mech.* **119**, 443-473.

Ho, C.-M. & Huerre, P. 1984 Perturbed Free Shear Layers. *Ann. Rev. Fluid Mech.* **16**, 365-424.

Huerre, P. & Monkewitz, P. 1990 Local and global instabilities in spatially developing flows. *Ann. Rev. Fluid Mech.* **22**, 473-537.

Hussain, A. K. M. F. & Zaman, K. B. M. Q. 1981 The 'preferred mode' of the axissymmetric jet. *J. Fluid Mech.* **110**, 39-71.

Koumoutsakos, P., Freund, J. B. & Parekh, D. 1998 Evolution strategies for parameter optimization in jet flow control. *Proceedings of the 1998 Summer Program,* Center for Turbulence Research, NASA/Stanford Univ., 121-132.

Koumoutsakos, P., Müller, S., Hilgers, A., Freund, J., & Parekh, D. 1999 Evolution strategies for jet mixing optimization. *IEEE Transactions on Evolutionary Computation,* (submitted).

Lee, M. & Reynolds, W. C. 1985 Bifurcating and blooming jets. *Report No. TF-22*, Department of Mechanical Engineering, Stanford University.

Mankbadi, R. R. 1985 The mechanism of mixing enhancement and suppression in a circular jet under excitation conditions. *Phys. Fluids* **28**, 2062-2074.

Michalke, A. 1984 Survey on jet instability theory. *Prog. Aerospace Sci.* **21**, 159-199.

Orlanski, I. 1976 A simple boundary condition for unbounded hyperbolic flows. *J. Comp. Physics* **21**, 251-269.

Parekh, D., Leonard, A., Reynolds, W. C., & M. G. Mungal 1987 Bifurcating of round air jets by dual-mode acoustic excitation. *AIAA Paper* 87-0164.

Parekh, D., Leonard, A.& Reynolds, W. C. 1988 Bifurcating jets at high Reynolds numbers. *Report TF-35* Department of Mechanical Engineering, Stanford University.

Parekh, D., Kibens, V., Glezer, A., Wiltse, J. M., & Smith, D. M. 1996 Innovative jet flow control: mixing enhancement experiments. 34th Aerospace Science Meeting, Reno, *AIAA Paper* 96-0308.

Rechenberg, I. 1994 Evolutionsstrategie - Optimierung technischer Systeme nach Prinzipien der biologischen Evolution. Fromann-Holzboog, Stuttgart.

Urbin G., Brun, C., & Métais, O. 1997 Large eddy simulation of three-dimensional spatially evolving round jets. in *11th Symposium on Turbulent Shear Flows*, Grenoble.